Available online at www.sciencedirect.com

ScienceDirect

IFAC PapersOnline CONFERENCE PAPER ARCHIVE

IFAC PapersOnLine 53-2 (2020) 1–6

Robust force control for brake-by-wire actuators via scenario optimization

Giorgio Riva, * **Dario Nava,** * **Simone Formentin,** * **Sergio M. Savaresi** *

* *Dipartimento di Elettronica, Informazione e Bioingegneria, Politecnico di Milano, Milan, Italy (e-mail: giorgio.riva@polimi.it).*

Abstract: Clamping force control in Electro Mechanical Brakes (EMBs) is a challenging task, mainly due to the nonlinear dynamics of the system and the uncertainty affecting its physical parameters. In this paper, a robust tuning of a PID control loop for an EMB is proposed. First, a control-relevant linear model of the system is derived. Then, the optimal parameters of the controller are tuned by solving a convex pole-placement problem and probabilistic robustness guarantees are provided according to the scenario theory. Finally, the performance of the proposed strategy is assessed on a complex nonlinear simulator of the EMB dynamics, and compared with the state of the art approach for robust control of EMBs.

1. INTRODUCTION

In recent years, the deployment of Drive-By-Wire technology in the automotive field has significantly grown, mainly due to its potential in vehicle dynamics control, e.g., through the coordination and integration of different vehicle actuators. In this context, the Electro Mechanical Brakes (EMBs) can be considered the state of the art technology for what concerns Brake-By-Wire (BBW) systems. In EMBs, the clamping force - namely the force exerted by the brake pads on the brake disk - is produced by an electric motor in series with a transmission/reduction stage, while the brake pedal plays the role of a mere sensor used to generate the clamping force set-point based on the driver pressure. The advantages carried by EMB technology w.r.t. the classic hydraulic brakes are several: (1) it allows to reduce the number of system components and overall weight, as well as to improve braking performance, by enabling individual control of each brake Line et al. (2008), (2) EMB actuators easily allow the integration with other by-wire devices, (3) EMB natively supports regenerative braking, which is an important feature in hybrid and electric vehicles Ahn et al. (2009).

The force control problem for EMB has been already addressed in previous works (see, e.g., Line et al. (2008),Jo et al. (2010),Line et al. (2004),Line et al. (2007)), but it is not yet solved, due to multiple issues. Firstly, critical problems arise in the development of control strategies due to the highly nonlinear behaviour exhibited by EMB over its range of operation. The causes of this behaviour can be attributed both to the nonlinear friction phenomena related to the transmission chain Jo et al. (2010),Kwak et al. (2004), also responsible for the possible occurrence of jammings of the mechanical system, and the nonlinear relationship (*i.e.* the so called characteristic curve Jo et al. (2010),Line et al. (2008)) between the clamping force and the EMB motor position. In order to manage these issues, in the scientific literature, different strategies have been proposed, such as gain scheduling Jo et al. (2010), feedforward compensation Line et al. (2008) and feedback linearisation Line et al. (2008),Line et al. (2007). Unfortunately, in all the above approaches, an accurate model of the EMB system is assumed to be available. Indeed, the physical parameters of EMBs are often uncertain and some of them (e.g., pad thickness and friction) may significantly vary throughout the BBW life cycle, mainly due to ageing and wear. As far as the authors are aware, the only work about a robust control strategy for EMBs is Line et al. (2007). Specifically, a robust high-order state-feedback H_∞ controller is considered, where a linear system with bounded uncertainty, obtained through preliminary feedback linearisation, is employed to describe the system dynamics.

The aim of this paper is to propose an alternative solution to the EMB robust control problem, where both the physical parameters and the operating point information are included in the system uncertainty description, and a simpler control architecture is employed. Specifically, unlike Line et al. (2007), this work is developed within a stochastic framework, endowing the uncertain parameters with specific probability density functions, and providing probabilistic guarantees via scenario optimization, see Calafiore and Campi (2006), Campi and Garatti (2018), Campi et al. (2009). Moreover, a fixed-structure controller, namely a PID, is employed and tuned through a pole placement approach, by keeping the overall system simple. The selected tuning method allows to exploit the convex formulation of scenario optimization, which is able to guarantee an a-priori selected level of robustness. A natural extension of the proposed approach regards the non-convex formulation proposed in Campi et al. (2018), which enlarges the class of possible optimization problems at the price of a weaker a-priori robustness guarantee.

The reminder of the paper is as follows. In Section 2, the EMB system is described using a lumped parameters, rigid, nonlinear model and the robust force control problem is formally stated. In Section 3, after a brief introduction about the Scenario approach, the addressed robust pole-placement method is described in detail. To this purpose, a control-relevant Linear Time Invariant (LTI) model of the system is derived and employed in the formulation of the convex optimization problem. Finally, Section 4 illustrates the performance of the proposed solution on the full nonlinear simulator and compares it with the benchmark approach proposed in Line et al. (2007).

2. SYSTEM DESCRIPTION AND PROBLEM STATEMENT

This section presents a description of the EMB actuator, together with a detailed nonlinear mathematical model, which

10.1016/j.ifacol.2020.12.025

will be employed as a system simulator in the remainder of the work. The addressed control problem is then defined, with a focus on the requirements and the description of the uncertainty.

2.1 System Description

The actuator can be decomposed, from an high level point of view, in three main parts, namely *driver interface*, *electrical part* and *mechanical part*, which are depicted in the schematic portray of Figure 1.

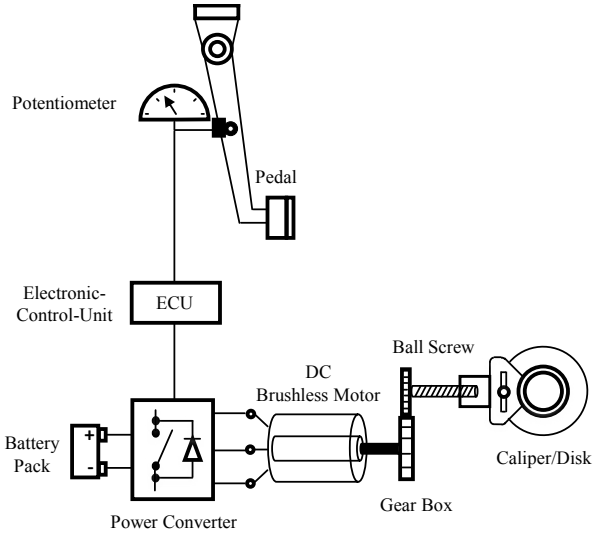

Fig. 1: EMB system overview. Three main parts can be distinguished: the driver's interface (pedal, potentiometer), the electric part (Battery Pack, ECU, Power Converter, DC Brushless Motor) and the mechanical part (gear box, ball screw, caliper/disk).

In particular, the interface links driver and actuation unit, and contrarily to a classic hydraulic actuator, where a pipeline connects directly driver and brake disk, introduces a complete disengagement. Indeed, the driver's braking request is read as a pedal position through a potentiometer and the information is transmitted to the Electronic-Control-Unit (ECU) of the vehicle.

At this level, we are looking for an I/O description of the system, so that, the interface is not taken into account. Indeed, we focus on the relationship between the duty cycle of the power converter, namely D_c, and the clamping force on the brake disk F_{cl}. Moreover, since we are interested in the principal dynamics of the system, simplifying assumptions will be taken, and motivated, in the next development.

According to Figure 1, the model is derived analysing separately electrical and mechanical parts, which are linked together through the motor. Notice that, for what concerns the former, the derivation detailed below is an extension of the one proposed in Line et al. (2008).

First of all, the electrical part is accounted for by means of a static relationship, thus neglecting the dynamics of both the converter and the motor current, which are commonly much faster than the mechanical dynamics. The converter is then considered as an ideal transformer with a variable, positive or negative, transformation ratio, namely the input duty cycle D_c. Moreover, the three phase DC Brushless motor is modelled as an equivalent DC motor (with resistance $R_m\,[\Omega]$ and torque/back EMF constant $K_m\,[\frac{Nm}{A}]$). Finally, two resistances, $R_1\,[\Omega]$ and $R_2\,[\Omega]$, are introduced to model the cabling between the battery source, i.e. V_b, and the power converter, and between the latter one and the motor.

Merging these modelling choices, the relationship between D_c and motor current i_m turns out to be:

$$i_m = \frac{D_c V_b - K_m \omega_m}{R_1 D_c^2 + R_2 + R_m} \tag{1}$$

In (1) the term $K_m\omega_m$ represents the back-EMF contribution, being ω_m the motor velocity. On the other side, the electrical subsystem affects the mechanical one through the electromechanical torque, obtained as $T_m = K_m i_m$.

Regarding the modelling of the mechanical part (see the block scheme in Figure 2), some assumptions are taken to obtain a fairly simple representation. In particular, the mechanical

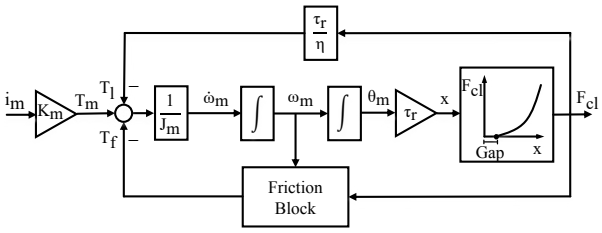

Fig. 2: Mechanical model describing the relationship between the motor current and the clamping force.

chain, from the motor shaft to the pads, is considered as a complete rigid body, neglecting elasticity. This simplification is confirmed by the dissertation proposed in Kwak et al. (2004), where the neglected phenomena are shown to be related to high frequency vibration modes, far from the level of accuracy of interest. Thus, the mechanical part is considered as a one-degree of freedom system, with a transmission between the motor and the load. Such a transmission is accounted for by means of the efficiency η and the reduction ratio $\tau_r\,[\frac{m}{rad}]$, transforming motor angular position θ_m into the linear one, i.e. x.

The following torque balance describes the general expression of this subsystem:

$$J_m \dot{\omega}_m = T_m - T_l - T_f, \tag{2}$$

where J_m represents the motor inertia, while T_l and T_f denote the load and friction torques, respectively. Despite the simplicity of Equation (2), complexity arises while expressing the torques. The former torque, i.e T_l, is given as follow:

$$T_l = \frac{1}{\eta}\tau_r F_{cl}(x) \tag{3}$$

As explained in Line et al. (2008), complexity lies in the expression of F_{cl}, which exhibits a cubic polynomial dependence on the pads position, together with a gap clearance between disk and pads x_{gap}. This behaviour is formalized in Equation (4), where $x^* = x - x_{gap}$:

$$\begin{cases} F_{cl} = 0, & x^* < 0 \\ F_{cl} = a_1 x^* + a_2 x^{*2} + a_3 x^{*3}, & x^* \geq 0 \end{cases} \tag{4}$$

The friction torque T_f, instead, is introduced through a classic model, including static (T_s), dynamic (T_c) and viscous (F_v) effects. In addition, static and dynamic parts are made load-dependent through a coefficient γ, as reported in the following expression (where $T_{ext} = T_m - T_l$):

$$\begin{cases} T_f = (T_c + \gamma F_{cl})sign(\omega_m) + F_v\omega_m, & \omega_m \neq 0 \\ T_f = \min(|T_{ext}|, T_s + \gamma F_{cl})sign(T_{ext}), & \omega_m = 0 \end{cases} \tag{5}$$

Equation (5) introduces a sharp discontinuity around zero speed, which makes the simulation complex and subject to

Table 1: Nominal values of physical model parameters.

Parameter	Value	Parameter	Value
$a_1\ [\frac{N}{mm}]$	1.038×10^4	$K_m\ [\frac{Nm}{A}]$	0.0195
$a_2\ [\frac{N}{mm^2}]$	2.58×10^4	$R_m\ [\Omega]$	0.1
$a_3\ [\frac{N}{mm^3}]$	-1.15×10^4	$R_1\ [\Omega]$	0.0194
$D_v\ [\frac{rad}{s}]$	0.01	$R_2\ [\Omega]$	0.05
$V_b\ [V]$	9	$T_s\ [Nm]$	0.03
η	0.93	$T_c\ [Nm]$	0.01
$\tau_r\ [\frac{m}{rad}]$	0.0241×10^{-3}	$F_v\ [\frac{Nms}{rad}]$	3×10^{-4}
$x_{gap}\ [mm]$	0.3275	$\gamma\ [\frac{Nm}{N}]$	1.26×10^{-5}
$J_m\ [kgm^2]$	5×10^{-6}		

chattering phenomena. This issue can be addressed in different ways (see Haessig and Friedland (1990)). In this work, the *Karnopp* remedy is employed, which defines a velocity band $\pm\, D_v$ within which the body is assumed to "stick" Haessig and Friedland (1990). For completeness, Table 1 reports the nominal values of the employed model parameters. The model developed here will be employed both as benchmark for the real system and as data generator in controller tuning and testing.

2.2 Problem Statement

The objective addressed in this work is the tuning of a fixed-structure force controller, which is also robust against parameters uncertainty. The controller is selected as the PID controller

$$R(s) = K_p + \frac{K_i}{s} + K_d \frac{s}{1 + \frac{s}{p_d}} \tag{6}$$

where, K_p, K_i and K_d represent respectively proportional, integral and derivative gains, while p_d takes the role of the high frequency pole, introduced to achieve feasibility.
The control specifications are given in terms of response time and bandwidth. In particular, the system is required to follow step references in $200\,[ms]$ (maximum) and to guarantee a bandwidth of at least $6-8\,[Hz]$. These requirements will be here addressed through a pole-placement approach.
Some parameters are assumed to be uncertain, in particular the motor resistance R_m, the torque constant K_m, the motor inertia J_m, the transmission efficiency η, the Coulomb friction T_c, the viscous friction F_v and the load dependent friction coefficient γ. Each of them is associated to a Gaussian distribution, centred around its nominal value (Table 1) and with standard deviation reported in Table 2. These latter values have been selected based on datasheet information about the electric motor and on a set of available external test for friction parameters. Such a stochastic system description has to be handled with probabilistic methods. In what follows, we will define scenario-based tools for our purposes.

3. SCENARIO-BASED CONTROL DESIGN

3.1 Scenario optimization and robust pole placement

A complete overview of scenario optimization can be found in Campi and Garatti (2018). The core of this approach is to handle robustness solving a convex optimization problem based on a finite number N of available samples, representing the overall uncertainty set. An important aspect is related to its probabilistic nature, since the employed scenarios have to be extracted independently from the uncertainty set, endowed with a probability description $\mathbb{P}$. The formalism employed in Campi and Garatti (2018) is here followed, thus an instance of uncertainty is denoted by δ and belongs to the uncertainty set Δ. Moreover, design parameters and performance index are labelled respectively with θ and $l(\theta,\delta)$.
Robustness is related to the probability of violation of a solution θ^*, called $V(\theta^*)$, (associated with an optimal performance index l^*), which is defined by the following equation:

$$V(\theta^*) = \mathbb{P}\{\delta \in \Delta :\ l(\theta^*,\delta) > l^*\} \tag{7}$$

The powerfulness of this approach is held by the so called *"Generalization Theorem"*, which defines a probabilistic guarantee about the solution of the optimization problem (where d represents the number of design variables):

$$\mathbb{P}^N\{V(\theta^*) > \varepsilon\} \leq \beta(N,\varepsilon,d) \tag{8}$$

where β represents the confidence level depending on the number of scenarios N, the risk level ε and d. During the design phase, ε and β are tuned in order to select a desired level of robustness. According to the selected values, the number of required scenarios can be computed directly from the bisection algorithm proposed in Campi and Garatti (2018).
Finally, this general approach can be particularized and employed to solve the problem discussed in Section 2. The robust-pole placement approach presented in Campi and Garatti (2018) is picked up and specialized. This method is proposed in a very general framework and requires only LTI descriptions of both uncertain plant $G(s,\delta)$ and controller $R(s)$. This generality allows an important degree of freedom, since it can be applied with different controller structures and plant models with respect to the ones employed here.

Table 2: Standard deviations of uncertain model parameters, as fractions (%) of the nominal values.

Parameter	Standard Deviation [%]
η	15
$J_m\ [kgm^2]$	10
$R_m\ [\Omega]$	12
$K_m\ [\frac{Nm}{A}]$	12
$T_c\ [Nm]$	15
$F_v\ [\frac{Nms}{rad}]$	15
$\gamma\ [\frac{Nm}{N}]$	10

3.2 Control-relevant modeling

In order to address the proposed method, a LTI uncertain model of the EMB is required. Indeed, the one developed in Section 2 includes important non-linearities, i.e. friction and clamping force expressions, and cannot be managed in the robust pole-placement framework. Thus, a simplified version is proposed, analysing the behaviour locally around a fixed operating condition.

The following considerations require some preliminary simplifications. Firstly, being the focus about force control, only the contact phase is considered, shifting the origin of the reference frame at the gap clearance distance. Then, the first cabling resistance, namely R_1, is left out, because its contribution in Equation (1) is assumed to be negligible. Moreover, friction expression is highly simplified, accounting only the linear viscous effect, as shown is Equation (9):

$$T_f = F_v \omega_m \tag{9}$$

Finally, Equation (2) has been linearised around a specific operating point, characterized by a constant position (i.e. force) value. In particular, clamping force can be approximated, around a position $\bar{x}$, as:

$$\begin{aligned} F_{cl} &\simeq F_{cl}(\bar{x}) + \left.\frac{dF_{cl}}{dx}\right|_{x=\bar{x}} (x-\bar{x}), \\ \left.\frac{dF_{cl}}{dx}\right|_{x=\bar{x}} &= \bar{k} = a_1 + 2a_2\bar{x} + 3a_3\bar{x}^2 \end{aligned} \tag{10}$$

Rearranging equations, the dynamic matrix of the linearised state-space model turns out to be the following, where the state vector is made up by motor position and speed:

$$A = \begin{bmatrix} 0 & 1 \\ \dfrac{-\tau_r^2 10^3 \bar{k}}{J_m \eta} & -\dfrac{F_v + \frac{K_m^2}{R_2+R_m}}{J_m} \end{bmatrix} \tag{11}$$

This derivation allows to figure out the characteristics about the eigenvalues of this approximated system, spanning the whole range of possible working conditions. In particular, the expression of the two time constants, considering the range of physical parameters described in Tables 1 and 2, are the following:

$$T_1 = \eta \frac{(F_v + \frac{K_m^2}{R_2+R_m})}{\tau_r 10^3 \bar{k}} \qquad T_2 = \frac{J_m}{F_v + \frac{K_m^2}{R_2+R_m}} \tag{12}$$

Two main considerations can be carried out: the system shows a second-order over-damped dynamics where only the slower time constant, i.e. T_1, depends from the operating condition, i.e. $\bar{k}$; moreover, T_1 and T_2 are significantly different in magnitude, so that the model can be locally considered - in the range of frequencies of interest - as a first order, depending on the operating condition and the physical parameters.

Having in mind the simplifications carried out to obtain the linearised model, especially regarding the friction phenomena, the results proposed in Equations (11) and (12) are only used to select an appropriate model structure, namely a first order system.

It follows that, a general expression of the control-oriented model, i.e. the transfer function between the control input D_c and the controlled variable F_{cl} depending on the uncertainty δ, is the following:

$$G(s,\delta) = \frac{k(\delta)}{s + p(\delta)}. \tag{13}$$

The choice to avoid the direct employment of the linearised system derived in Equation (10) is motivated also by the availability of a simulator of the nonlinear system, which can be directly used to perform ad-hoc identification experiments, accounting the effect of friction. More specifically, identification of Equation (13) is carried out by means of small amplitude step perturbations, of the control variable D_c, around a selected working condition, fitting the model on the resulting response thorough classical techniques based on step response.

As a consequence of this modelling choice, Equation (13) has only local validity, so that the working point has to be accounted. This fact has been addressed including it in the list of the uncertain parameters. More specifically, a uniformly distributed force working condition $\bar{F} \in [\,0\,,\, F_{max}\,]$ is considered (where F_{max} depends from the specific actuator, e.g. $20\,[kN]$ in this example).

Figure 3 shows a comparison of a step response between four identified LTI models and their non linear counterparts around a working condition, where both models parameters and operating points have been generated according to the probabilistic setup previously described.

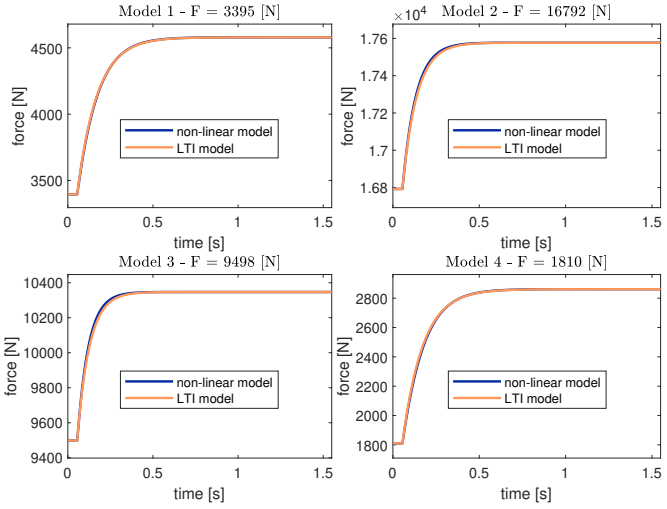

Fig. 3: Validation of the proposed modeling approximation. Comparison between the step response of the nonlinear model and the identified first order LTI system in four different scenarios, i.e. with random gaussian parameters and uniformly distributed force working conditions (F).

3.3 Implementation

Finally, having LTI formulations of both plant and controller, the robust pole-placement method can be specialized on the problem at hand. More precisely, the closed-loop system turns out to be a third-order, whose characteristic polynomial can be generally expressed as follow:

$$p_{cl}(s) = s^3 + r_2 s^2 + r_1 s + r_0 \tag{14}$$

In our specific case, Equation (14) is specialized as a function of model (δ) and controller ($\theta = |K_p\, K_i\, K_d|$) parameters, as shown in Equation (15):

$$\begin{aligned} p_{cl}(s,\theta,\delta) = s^3 + r_2(\theta,\delta)s^2 + r_1(\theta,\delta)s + r_0(\theta,\delta) = \\ s^3 + (p(\delta) + p_d + K_p k(\delta) + K_d k(\delta) p_d)s^2 + \\ + (p(\delta)p_d + K_i k(\delta) + K_p k(\delta) p_d)s + K_i k(\delta) p_d \end{aligned} \tag{15}$$

The cost function is selected as the sum of the distances, in absolute value, between the coefficients of the desired characteristic polynomial, named r_2^*, r_1^*, r_0^*, and the ones expressed in Equation (15), represented by terms $r_2(\theta,\delta)$, $r_1(\theta,\delta)$, $r_0(\theta,\delta)$:

$$l(\theta,\delta) = |r_2^* - r_2(\theta,\delta)| + |r_1^* - r_1(\theta,\delta)| + |r_0^* - r_0(\theta,\delta)| \tag{16}$$

As a consequence, the overall optimization problem reads:

$$\min_{\theta=|K_p,K_i,K_d|} \max_{i=1,\dots,N} l(\theta,\delta_i) \tag{17}$$

where N is the number of scenarios considered. As a remark, the choice of this particular cost function is grounded on its

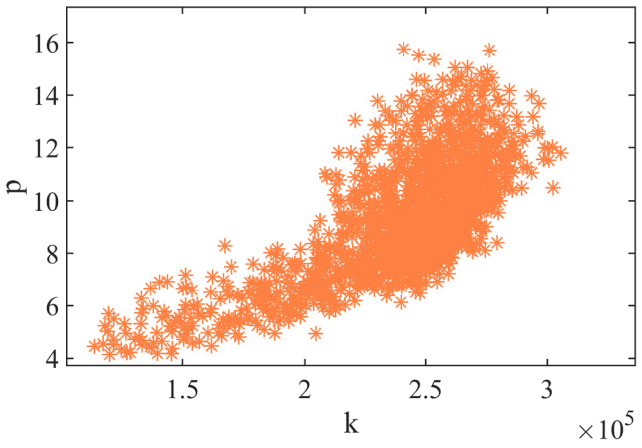

Fig. 4: Extracted scenarios: each marker in (k,p) plane represents one LTI uncertain model employed in the optimization.

convexity property. Indeed, different measures would lead to a non-convex optimization problem, such as minimizing the distances in the complex plane between the poles and their desired locations, which attains weaker a-priori robustness properties. Moreover, the selected performance index is slightly different from the one proposed in Campi and Garatti (2018). This choice was made to enforce the uniqueness of the solution, since it may be not guaranteed with specific combinations of controller structures, plants and requirements.
Finally, we want to remind that the min/max optimization problem defined by Equation (17) can be rewritten as a single minimization problem by means of an additional slack variable, as explained in Campi et al. (2009), and solved through standard convex optimization tools.

4. SIMULATION RESULTS

In this final section, the proposed solution is implemented in simulation. According to the overall uncertainty description, each scenario is obtained extracting a set of physical parameters and one working condition $\bar{F}$, around which the model defined in Equation (13) can be identified (as described in the final part of Section 3.2).
Moreover, as anticipated in Section 3, two design parameters have to be chosen to select a desired level of robustness. In this example, ε and β are set respectively equal to 1% and 0.01%, since, as explained in Calafiore and Campi (2006), the confidence level can be assigned close to one without a significant increase in the number of samples. Moreover, the number of design parameters is $d = 4$, due to the introduction of the slack variable . By means of the mentioned bisection algorithm and the selected tuning parameters the number of samples results $N = 1585$. Thus, N control-oriented models are obtained, which are depicted, as a cloud of points in the (k, p) plane, in Figure 4.
Lastly, control specifications defined in Section 2 has to be translated in the pole-placement framework, namely defining the desired closed-loop pole. In this specific case, two of them are selected in order to satisfy, with a reasonable margin, the bandwidth requirement (which is compatible with response time), namely $p_{cl1} = p_{cl2} = 2\pi 15\ [\frac{rad}{s}]$, while the remaining one is placed at higher frequency, i.e. $p_{cl3} = 2\pi 80\ [\frac{rad}{s}]$. As a consequence, the desired closed-loop characteristic polynomial turns out to be:

$$p_{cl}(s) = s^3 + 691.15\, s^2 + 1.0363 \times 10^5\, s + 4.465 \times 10^6 \quad (18)$$

As final remark, the derivative filter p_d is fixed equal to 120, placed at higher frequency with respect to the dominant closed-loop poles.
Now that all the ingredients of Equation (17) are defined, the convex optimization problem can be solved. Table 3 reports the optimal controller parametrization and achieved optimal value of the cost function (l^*), namely the slack variable.

Table 3: Optimal PID gains and Cost Function.

$K_p^*\ [\frac{1}{N}]$	$K_i^*\ [\frac{1}{Ns}]$	$K_d^*\ [\frac{s}{N}]$	l^*
0.0038	0.1763	1.0706×10^{-5}	2.09×10^6

An a-posteriori validation of the violation probability is performed, testing the optimal controller parametrization with a new set of control-oriented models N^*. Violation is defined to be the event in which the performance index, computed with a new instance, exceeds the optimal bound achieved from optimization, namely l^* in Table 3. Thus, an estimation of the probability of violation of the optimal solution $\hat{\varepsilon}$ can be estimated as the percentage of times the performance is violated using the new set of models over N^*. In this example, the number of new instances is selected equal to the optimization one, namely 1585, and the corresponding estimated probability of violation results $\hat{\varepsilon} = 0.063\ \%$, which is smaller than the desired one, confirming the level of robustness guaranteed by the Scenario approach with almost unitary confidence (see Equation (8)).
In this last part of the section, an evaluation about performance and robustness is carried out by testing the achieved controller on the non-linear model introduced in Section 2. To enrich the analysis, results are compared with the benchmark method of Line et al. (2007), adapted to cope with the structured controller proposed in this work, namely a PID. To this purpose, feedback linearisation and inverse gain scheduling compensations are implemented as proposed in Line et al. (2007), then structured H_∞ synthesis is performed using the MATLAB® `hinfstruct` function, see Gahinet and Apkarian (2011). Concerning the uncertainty description, the parameters remaining after feedback linearisation are bounded by one and half the standard deviations reported in Table 2, while the remaining ones are embedded through additional uncertainty terms modelling compensation errors. Finally, as proposed in Line et al. (2007), performance requirements are addressed shaping the sensitivity function, carrying out two different tuning selections. We want to remark that, because the two approaches are considerably different, performance specifications can be only qualitatively compared.
During the following analysis, $N = 10$ model parametrizations are considered, here again extracted from the same probabilistic description, making a compromise between generality and readability of the results. In order to highlight control requirements in the whole operating region, a set of step references is chosen to test the systems, namely $2500\,/\,5000\,/\,7500\,/\,10000\,/\,15000\,/\,20000\ [N]$.
It is important to point out that, the control variable, i.e. D_c, is saturated between $[-1, 1]$ to account for physical limitations of the power supply. As a consequence, the PID controllers are implemented in their typical anti wind-up configuration.
Simulation results are reported in Figure 5. Specifically, in Figure 5a, the scenario optimization solution is compared with a more aggressive tuning of the H_∞ controller, while Figure

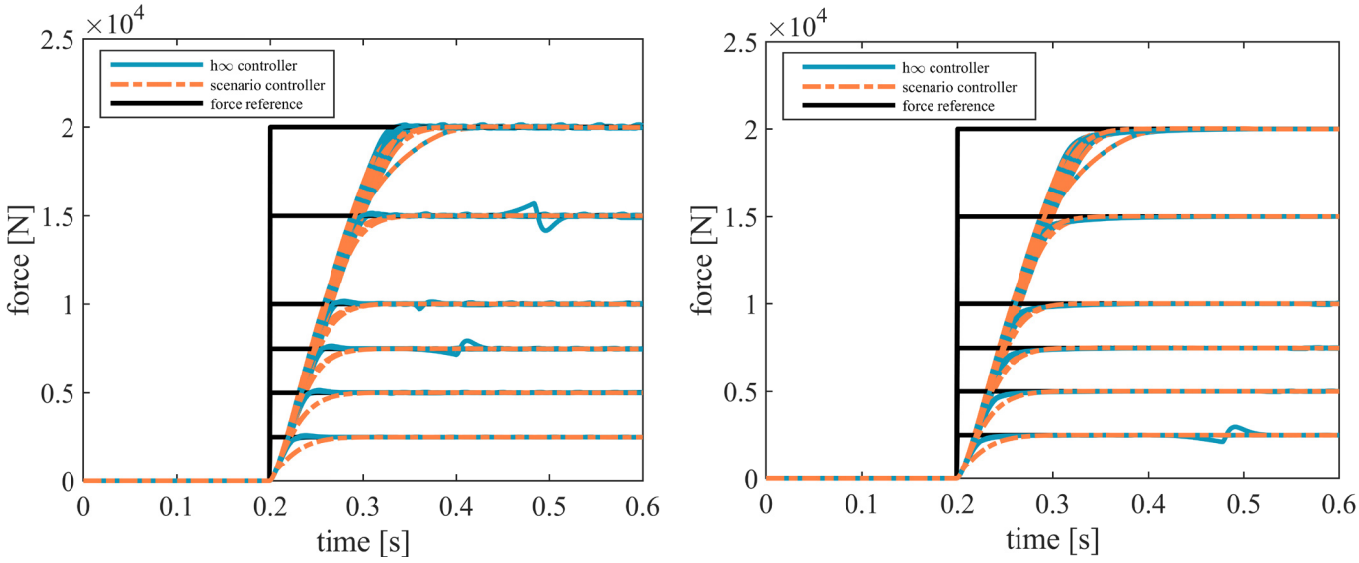

(a) scenario vs. aggressive H_∞

(b) scenario vs. conservative H_∞

Fig. 5: Simulation results on the nonlinear model comparing scenario and H_∞ solutions, for different step excitations for 10 model parametrizations.

5b shows a more conservative synthesis. The scenario PID controller satisfies the desired response time for all considered uncertain systems and operating conditions. The responses slow down when higher references are fed, which can be ascribed partly to actuator saturation. At the same time, it carries a positive effect, avoiding overshoots in the response. Concerning the H_∞ approach, notice that the aggressive controller shows faster responses *w.r.t.* scenario ones, especially for low target forces, also thanks to the presence of the inverse gain scheduling. At the same time, friction compensation may generate oscillations around steady-state conditions, that are clearly visible in Figure 5a. The conservative tuning, instead, shows comparable responses with the scenario solution (see Figure 5b).
To summarize, the compared approaches qualitatively show similar performance, even though the scenario-based one relies on a simpler controller architecture and its tuning procedure is computationally less demanding.

5. CONCLUSIONS

In this paper, a probabilistic solution for the robust force control of a BBW actuator is discussed, grounded on scenario optimization techniques. More precisely, an uncertain LTI control-relevant model is derived from a non-linear simulator and employed in a pole-placement convex optimization environment to tune a PID controller. Simulation results show satisfactorily performance as compared to the benchmark H_∞ robust controller. Future work will be devoted to the experimental validation of the proposed approach and to the development of extensions about the employed methodology.

REFERENCES

Ahn, J.K., Jung, K.H., Kim, D.H., Jin, H.B., Kim, H.S., and Hwang, S.H. (2009). Analysis of a regenerative braking system for hybrid electric vehicles using an electro-mechanical brake. *International Journal of Automotive Technology*, 10(2), 229–234.

Calafiore, G.C. and Campi, M.C. (2006). The scenario approach to robust control design. *IFAC Proceedings Volumes*, 39(9), 602 – 607. 5th IFAC Symposium on Robust Control Design.

Campi, M. and Garatti, S. (2018). *Introduction to the Scenario Approach*. Society for Industrial and Applied Mathematics, Philadelphia, PA.

Campi, M.C., Garatti, S., and Ramponi, F.A. (2018). A general scenario theory for nonconvex optimization and decision making. *IEEE Transactions on Automatic Control*, 63(12), 4067–4078.

Campi, M.C., Garatti, S., and Prandini, M. (2009). The scenario approach for systems and control design. *Annual Reviews in Control*, 33(2), 149 – 157.

Gahinet, P. and Apkarian, P. (2011). Structured h-inf synthesis in matlab. *IFAC Proceedings Volumes*, 44(1), 1435–1440.

Haessig, D. and Friedland, B. (1990). On the modeling and simulation of friction. volume 1482, 1256 – 1261.

Jo, C., Hwang, S., and Kim, H. (2010). Clamping-force control for electromechanical brake. *IEEE Transactions on Vehicular Technology*, 59(7), 3205–3212.

Kwak, J., Yao, B., and Bajaj, A. (2004). Analytical model development and model reduction for electromechanical brake system.

Line, C., Manzie, C., and Good, M.C. (2008). Electromechanical brake modeling and control: From pi to mpc. *IEEE Transactions on Control Systems Technology*, 16(3), 446–457.

Line, C., Manzie, C., and Good, M. (2004). Control of an electromechanical brake for automotive brake-by-wire systems with an adapted motion control architecture. volume 113.

Line, C., Manzie, C., and Good, M. (2007). Robust control of an automotive electromechanical brake. *IFAC Proceedings Volumes*, 40(10), 579 – 586. 5th IFAC Symposium on Advances in Automotive Control.